International Journal of Heat and Mass Transfer 227 (2024) 125576

Contents lists available at ScienceDirect

International Journal of Heat and Mass Transfer

journal homepage: www.elsevier.com/locate/ijhmt

The influence of thermal diffusion on water migration through a porous insulation material

Vegard G. Jervell [a], Magnus Aa. Gjennestad [b], Thuat T. Trinh [a], Øivind Wilhelmsen [a,b,*]

[a] Porelab, Department of Chemistry, Norwegian University of Science and Technology, Høgskoleringen 5, Trondheim, Norway
[b] SINTEF Energy Research, Sem Sælands vei 11, Trondheim, Norway

ARTICLE INFO

Keywords:
Porous media
Porosity
Water
Corrosion under insulation
Non-equilibrium thermodynamics
Nonisothermal

ABSTRACT

Excess water on pipes and equipment under porous insulation materials can lead to undesired corrosion. This work aims to clarify to what extent thermal diffusion affects the migration of water inside insulation materials subject to large temperature gradients. Since no experimental data is available on the thermal diffusion coefficients of humid air, revised Enskog theory for Mie fluids is used to estimate transport properties. Comparison to experimental data from literature shows that the theory reproduces the diffusion coefficient, viscosity and thermal conductivity of humid air within 8.7%, 5.0% and 3.5% respectively. The small discrepancies suggest that the theory can also provide reliable estimates of the thermal diffusion coefficients. In the investigated composition and temperature range, the theory predicts the Soret coefficient of water to be approximately $-0.3\,\mathrm{mK}^{-1}$, while the Soret coefficient of oxygen varies from $-1.2\,\mathrm{mK}^{-1}$ to $+0.1\,\mathrm{mK}^{-1}$. A case study with heating of glass wool insulation containing humid air, encapsulating a cylindrical pipe is investigated. Non-equilibrium thermodynamics is used to consistently incorporate the Soret coefficients into the flux equations in a dynamic, non-isothermal model that includes diffusion, convection, thermal conduction and water sorption in the porous medium. With 50 K temperature difference across 5 cm of insulation, we find that at steady-state, thermal diffusion leads to a mole fraction of water in the gas phase that is about 1.5% higher at the hot location than if thermal diffusion is neglected.

1. Introduction

The water molecules contained in air are frequently referred to as *moisture* [1]. Moisture in building materials is one of the major causes of degradation and reduction of thermal performance [2]. Therefore, the coupling between heat and moisture transfer in building materials has been an active research topic for many years [2–6]. Both experimental [6] and numerical [7] efforts have shed light on how the moisture migrates, while at the same time interacting with an adsorbed water phase inside the porous material. In the study of building materials, the thermal driving force is mainly limited by variations in the ambient temperature and heat ingress from the sun by radiation [8]. Other applications such as drying [9] e.g. of textiles [10], or in production of paper [11] or fuel cells [12], the thermal driving force can be much larger. Another application with potential for very high temperature gradients is the inside of porous insulation materials around hot pipes or process equipment [13]. The extent to which large temperature gradients influence the migration of water is important to clarify, since excess water under the insulation can lead to corrosion [14,15]. The simultaneous coexistence of multiple phases in the presence of a large temperature gradient gives the possibility for several transport phenomena to occur, such as evaporation/condensation, capillary effects [16–18] and thermal diffusion [19–21].

A simple description of diffusive mass transfer is provided by Fick's law, which states that the diffusion flux goes in the opposite direction of the concentration gradient [22]. Unless this formulation is extended, it will give incorrect results in systems subject to a large temperature gradient [23,24].

Fourier's law is an analogous description of heat transfer, which states that the heat flux moves in the opposite direction of the temperature gradient [24]. Supplementary to these laws, Ludwig (and later Soret) showed in 1856 that a temperature gradient can induce a mass

* Corresponding author.
E-mail address: oivind.wilhelmsen@ntnu.no (Ø. Wilhelmsen).

https://doi.org/10.1016/j.ijheatmasstransfer.2024.125576
Received 12 January 2024; Received in revised form 22 March 2024; Accepted 15 April 2024
Available online 24 April 2024

flux [25,26]. This is called the Soret effect or thermal diffusion. A concentration gradient can also induce a heat flux (the Dufour effect) [24]. These phenomena are linked and referred to as coupled transport processes [27]. Thermal diffusion has been hypothesized to play an important role in e.g. drying of porous media [9], where moisture is transported out of the material.

The magnitude of the coupling between heat and mass transfer is quantified by the Soret coefficient. Several works have been devoted to determining the value of the Soret coefficient in a variety of systems, by use of models [19,28–30], and measurements [31–33]. It is important to clarify the impact of thermal diffusion on transport through porous media [20,34,35]. In particular, the role of thermal diffusion in the migration of water in humid air through porous insulation materials subject to large temperature gradients, remains a knowledge gap. A key challenge in this regard is that the value of the thermal diffusion coefficient of water in air has, to the best of our knowledge, not yet been measured. In this work, we present the first estimates of the Soret coefficients of the components of air predicted with revised Enskog theory [36].

In a paper from 2011 [37], Janssen discusses previous experimental investigations of porous insulation materials where thermal diffusion has been hypothesized to be present or not [38,39]. He comes to the conclusion that previous measurements can be explained without considering thermal diffusion. He argues that at least in building physics: "vapor pressure is the sole significant transport potential for the diffusion of water vapor in porous media". On the other hand, Häussling, Löwgren and colleagues [9] claim that thermal diffusion is an important effect to consider in drying, where the temperature gradients are likely to be larger than in building physics. In this work, we aim to contribute to this discussion by 1) Providing the first reliable estimates of the Soret coefficients of humid air, 2) Estimating their influence on moisture transport in a porous insulation material subject to a large temperature gradient.

The paper will be structured as follows. We provide the underlying balance equations for transport of heat, mass and momentum in the porous medium in Sec. 2. Here, we will also provide closure relations to these balance equations by use of non-equilibrium thermodynamics. Details on how the equations have been solved numerically and description of the methodology can be found in Sec. 3. A discussion of thermal diffusion and its influence on the case considered can be found in Sec. 4 and concluding remarks are provided in Sec. 5.

2. Theory

We present the governing balance equations for the porous insulation material in Sec 2.1, including the expression for the local entropy production. Next, the local entropy production is used to formulate consistent force-flux expressions in Sec. 2.2. We connect the solutions from revised Enskog theory to the Onsager coefficients in force-flux relations from non-equilibrium thermodynamics in Sec. 2.3.

2.1. General transport equations and entropy production

In this section, we shall state the balance equations used to model transport through the porous medium. They are identical to those used in [40] and are summarized here for completeness.

The porous medium contains three phases, a solid phase (s), a gaseous phase (g) and an adsorbed phase (a), and we assume local thermal, chemical and mechanical equilibrium between them. While the gas can be a mixture of different chemical components, the adsorbed phase is here assumed to be pure and we use the thermodynamically consistent model from [40] to describe it. The solid is assumed to be stagnant, chemically inert, and incompressible, so that the solid density ρ^{s} is constant and known. Also, the porosity is assumed known. The employed transport equations treat the different phases as interpenetrating continua, i.e. all three phases may be present at any given point in space. They are therefore applicable at length scales much larger than the typical pore size. Furthermore, the transport equations are formulated on a mass basis and we therefore use mass-based quantities for, e.g., chemical potential, entropy and enthalpy, rather than molar quantities, in this section.

The mass balance for each component i in each phase j is

$$\partial_t \left\{ \alpha^j \rho^j w_i^j \right\} + \nabla \cdot \left\{ \alpha^j \boldsymbol{j}_i^j \right\} = \Psi_i^j, \tag{1}$$

where α^j is the volume fraction of phase j, w_i^j is the mass fraction of component i in phase j, ρ^j is the mass density of phase j and Ψ_i^j accounts for mass transfer between phases. Since we assume that the adsorbed phase is pure, and therefore consists of Component 1 only, then $\Psi_1^{\mathrm{g}} = -\Psi^{\mathrm{a}}$ and $\Psi_{i\neq 1}^{\mathrm{g}} = 0$.

The flux of component i through phase j is $\boldsymbol{j}_i^j$. This is composed of an advective and a diffusive part,

$$\boldsymbol{j}_i^j = w_i^j \rho^j \boldsymbol{v}_i^j = \bar{\boldsymbol{j}}_i^j + \tilde{\boldsymbol{j}}_i^j, \tag{2}$$

where $\bar{\boldsymbol{j}}_i^j = w_i^j \rho^j \boldsymbol{v}^j$ is the advective part, $\tilde{\boldsymbol{j}}_i^j$ is the diffusive part, also known as the barycentric mass flux, and $\rho^j \boldsymbol{v}^j = \sum_i w_i^j \rho^j \boldsymbol{v}_i^j$. Summing over all components, the mass balance of phase j is

$$\partial_t \left\{ \alpha^j \rho^j \right\} + \nabla \cdot \left\{ \alpha^j \rho^j \boldsymbol{v}^j \right\} = \Psi^j, \tag{3}$$

where $\Psi^j = \sum_i \Psi_i^j$.

The momentum balance for the gas phase is expressed (in component notation) as

$$\partial_t \left\{ \alpha^{\mathrm{g}} \rho^{\mathrm{g}} v_k^{\mathrm{g}} \right\} + \partial_m \left\{ \alpha^{\mathrm{g}} \rho^{\mathrm{g}} v_k^{\mathrm{g}} v_m^{\mathrm{g}} \right\} + \alpha^{\mathrm{g}} \partial_k \left\{ p \right\} = \alpha^{\mathrm{g}} \rho^{\mathrm{g}} g_k + \Theta_k^{\mathrm{g}} + v_k^{\mathrm{i}} \Psi^{\mathrm{g}}. \tag{4}$$

Herein, p is the pressure, g_k is the k-component of the gravitational acceleration, Θ_k^j represents the dissipative viscous friction forces acting on phase j in direction k and v_k^{i} accounts for the momentum transfer associated with mass transfer between the fluid phases. We choose here to set $v_k^{\mathrm{i}} = \left\{ v_k^{\mathrm{a}} + v_k^{\mathrm{g}} \right\}/2$, since this choice does not dissipate total kinetic energy.

The momentum balance of the adsorbed phase is similar, but has an additional term involving the spreading pressure φ,

$$\begin{aligned} &\partial_t \left\{ \alpha^{\mathrm{a}} \rho^{\mathrm{a}} v_k^{\mathrm{a}} \right\} + \partial_m \left\{ \alpha^{\mathrm{a}} \rho^{\mathrm{a}} v_k^{\mathrm{a}} v_m^{\mathrm{a}} \right\} + \alpha^{\mathrm{a}} \partial_k \left\{ p \right\} + a^{\mathrm{s}} \partial_k \left\{ \varphi \right\} \\ &\quad = \alpha^{\mathrm{a}} \rho^{\mathrm{a}} g_k + \Theta_k^{\mathrm{a}} + v_k^{\mathrm{i}} \Psi^{\mathrm{a}}. \end{aligned} \tag{5}$$

Herein a^{s} is the solid surface area per volume in the porous medium.

The balance equation for the total enthalpy $\rho h = \sum_j \alpha^j \rho^j h^j$, is

$$\begin{aligned} &\partial_t \left\{ \rho h \right\} + \partial_k \sum_{j\in\{\mathrm{g,a}\}} \left\{ \alpha^j \rho^j h^j v_k^j \right\} + \partial_k \sum_j \left\{ \alpha^j q_k^j \right\} \\ &\quad = \partial_t \left\{ p \right\} + \sum_{j\in\{\mathrm{g,a}\}} \left\{ \alpha^j v_k^j \partial_k \left\{ p \right\} - v_k^j \Theta_k^j \right\} \\ &\qquad + a^{\mathrm{s}} \partial_t \left\{ \varphi \right\} + a^{\mathrm{s}} v_k^{\mathrm{a}} \partial_k \left\{ \varphi \right\}, \end{aligned} \tag{6}$$

where $\boldsymbol{q}^j$ is the heat flux through phase $j \in \{\mathrm{g,a}\}$. For the gas phase, it may be expressed as

$$\boldsymbol{q}^{\mathrm{g}} = \tilde{\boldsymbol{q}}^{\mathrm{g}} + \sum_{i=1}^{N} h_i^{\mathrm{g}} \tilde{\boldsymbol{j}}_i^{\mathrm{g}}, \tag{7}$$

where $\tilde{\boldsymbol{q}}^{\mathrm{g}}$ is the measurable heat flux and h_i^{g} is the partial molar enthalpy. For the adsorbed and solid phases,

$$\boldsymbol{q}^j = \tilde{\boldsymbol{q}}^j. \tag{8}$$

In another work [40], we used the balance equations presented above to derive the expression

$$\sigma = \nabla \left\{ \frac{1}{T} \right\} \cdot \tilde{\boldsymbol{q}}^{\mathrm{tot}} + \sum_{i=1}^{N} \left(-\frac{\nabla_T \mu_i}{T} \right) \cdot \tilde{\boldsymbol{j}}_i^{\mathrm{tot}} - \sum_{j\in\{\mathrm{g,a}\}} \frac{v_k^j \Theta_k^j}{T} \tag{9}$$

for the local entropy production, σ, where $\tilde{\boldsymbol{j}}_i^{\text{tot}} = \alpha^{\text{g}}\tilde{\boldsymbol{j}}_i^{\text{g}}$ is the *total* barycentric mass flux of component i and $\tilde{\boldsymbol{q}}^{\text{tot}} = \sum_{j\in\{\text{g,a,s}\}} \alpha^j \tilde{\boldsymbol{q}}^j$ is the *total* measurable heat flux. Furthermore, the subscript T is used to indicate that the temperature should be held constant when taking the gradient.

The mass fluxes are subject to the constraint

$$\sum_{i=1}^{N} \tilde{\boldsymbol{j}}_i^{\text{tot}} = 0, \tag{10}$$

which can be used to reduce the number of driving forces. We may therefore reformulate the entropy production as

$$\sigma = \nabla\left\{\frac{1}{T}\right\}\cdot\tilde{\boldsymbol{q}}^{\text{tot}} + \sum_{i=1}^{N-1}\left(-\frac{\nabla_T\Psi_i}{T}\right)\cdot\tilde{\boldsymbol{j}}_i^{\text{tot}} - \sum_{j\in\{\text{g,a}\}}\frac{v_k^j\Theta_k^j}{T}, \tag{11}$$

where

$$\Psi_i = \mu_i - \mu_N. \tag{12}$$

2.2. Flux expressions from non-equilibrium thermodynamics

Based on Eq. (11) we formulate the constitutive force-flux relations

$$\tilde{\boldsymbol{q}}^{\text{tot}} = L_{q,q}\nabla\left\{\frac{1}{T}\right\} - \sum_{i=1}^{N-1} L_{q,i}\frac{1}{T}\nabla_T\Psi_i \tag{13}$$

$$\tilde{\boldsymbol{j}}_1^{\text{tot}} = L_{1,q}\nabla\left\{\frac{1}{T}\right\} - \sum_{i=1}^{N-1} L_{1,i}\frac{1}{T}\nabla_T\Psi_i \tag{14}$$

$$\vdots$$

$$\tilde{\boldsymbol{j}}_{N-1}^{\text{tot}} = L_{N-1,q}\nabla\left\{\frac{1}{T}\right\} - \sum_{i=1}^{N-1} L_{N-1,i}\frac{1}{T}\nabla_T\Psi_i \tag{15}$$

for heat and mass transfer in a mixture of N components. Here, $L_{k,z}$ are called Onsager coefficients. An advantage of using non-equilibrium thermodynamics, is that we can make use of the Onsager relations, which state that $L_{k,z} = L_{z,k}$. Due to the high porosity, and assuming that all mass transport takes place in the gas-phase, the Onsager coefficients in a porous medium can be modeled as

$$L_{k,z} \approx \alpha^{\text{g}} b_{k,z} L_{k,z}^{\text{g}} \quad \text{if} \quad k,z \neq q,q \tag{16}$$

where the positive phase-dependent constant $b_{k,z} \leq 1$ takes into account that, e.g., diffusion in a porous medium differs from that in a bulk gas (superscript g) due to steric hindrance. Furthermore, we have that:

$$L_{q,q} = T^2\left(\alpha^{\text{s}}\lambda^{\text{s}} + \alpha^{\text{a}}\lambda^{\text{a}}\right) + \alpha^{\text{g}}L_{q,q}^{\text{g}} \tag{17}$$

2.3. Transport properties from revised Enskog theory

The Enskog solutions of the Boltzmann equation in kinetic gas theory represent a powerful tool to investigate the behavior of dilute gases, where it has been shown to give accurate predictions [41–48]. Shortly after the Enskog solutions were presented, an extension of the theory to account for the covolume of hard sphere particles was developed for pure fluids [49,50]. Later, an extension to multicomponent mixtures of hard spheres was obtained [51–54]. These solutions were termed Revised Enskog Theory (RET), and extend the solution of the Boltzmann equation to higher densities.

We recently presented a RET for Mie fluids (RET-Mie) [36,55]. With Mie fluid parameters fitted to equilibrium properties, the theory is fully predictive for transport properties [36]. We showed that the theory accurately reproduces experimental values for diffusion coefficients, thermal conductivities, viscosities and thermal diffusion coefficients of several mixtures.

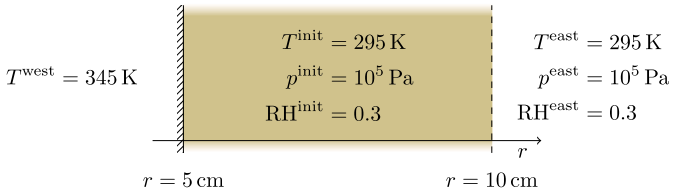

Fig. 1. Schematic illustration of boundary and initial conditions of the investigated case. Initially, the porous insulation has a temperature of 295 K, a relative humidity of 0.3 and pressure of 10^5 Pa. The right side is open towards ambient air with temperature, pressure and relative humidity equal to the initial values. The left side of the domain is a wall with constant temperature of 345 K.

In this work, we connect the framework of RET to the Onsager coefficients in non-equilibrium thermodynamics in order to predict the transport properties of humid air. We find that

$$L_{i,j}^{\text{g}} = \frac{x_i M_i d_{i,j}^{(0)} x_j M_j}{2N_A R},$$

$$L_{i,q}^{\text{g}} = -RT\sum_{j=1}^{N-1} L_{i,j}^{\text{g}}\left(\frac{1-k_{T,j}}{M_j} - \frac{1-k_{T,N}}{M_N}\right), \tag{18}$$

$$L_{q,q}^{\text{g}} = T^2\lambda^{\text{g}} - RT\sum_{i=1}^{N-1} L_{q,i}^{\text{g}}\left(\frac{1-k_{T,i}}{M_i} - \frac{1-k_{T,N}}{M_N}\right),$$

where R is the universal gas constant, M_i denote the molar masses, x_i is the mole fraction of component i, N_A is Avogadro's number, λ^{g} is the thermal conductivity of the gas phase, $d_{i,j}^{(0)}$ are the diffusive response functions' Sonine polynomial expansion coefficients, and $k_{T,i}$ are the thermal diffusion ratios as defined in Ref. [36]. A detailed derivation of Eq. (18) and more information can be found in the Supplementary Information (SI).

3. Methodology

3.1. The investigated case

To gain insight into the role of thermal diffusion in porous insulation materials subject to large temperature gradients, we will consider an example with heating of a humid insulation material surrounding a hot, cylindrical pipe. A schematic illustration of the example can be found in Fig. 1. At $t = 0$, the insulation material has uniform temperature ($T^{\text{init}} = 295$ K) and relative humidity ($\text{RH}^{\text{init}} = 0.3$) profiles. At $t = 0$, the temperature at the left boundary is increased to ($T^{\text{west}} = 345$ K), which causes moisture to redistribute inside the insulation material. In Sec. 4, we will investigate how thermal diffusion influences this redistribution process.

An important physical phenomenon to account for in insulation materials is the adsorption of water onto and into the porous matrix and we will perform simulations both with and without this effect. To have a concrete example for numerical calculations with adsorption, we will apply the thermodynamic framework to the well-known Brunauer-Emmett-Teller (BET) adsorption model for single-component adsorption [56,57]. We assume that the adsorption is independent of temperature [40], such that

$$\Gamma(\text{RH}) = \frac{a\xi\cdot\text{RH}}{\{1-c\cdot\text{RH}\}\{1-\text{RH}+\xi\cdot\text{RH}\}}. \tag{19}$$

We have used the constant $c = 1 - \frac{a}{\Gamma_\infty}$, which is smaller than, but very close to 1, which ensures that $\Gamma(\text{RH}=1,T) = \Gamma_\infty$. Using an area per adsorbed molecule of 0.3 nm^2, and fitting the parameters in Eq. (19) to the L2 data set from Ref. [58] for glass wool results in the parameters $a = 0.18\,\text{mol}\,\text{cm}^{-2}$, $c = 0.999$ and $\xi = 1388$ (average absolute relative deviation of 9.8 %), so that the adsorption area per volume of insulation is $a^{\text{s}} = 6.39\times10^5\,\text{m}^2\,\text{m}^{-3}$.

Both the liquid and solid phases are approximated as incompressible and the air is treated as an ideal gas mixture with three-components: water, nitrogen and oxygen.

We will consider a one-dimensional, horizontal case with full radial symmetry, and therefore set the gravitational acceleration to zero. The adsorbed phase is furthermore assumed not to flow, so that $j^{a}_{H_2O} = \mathbf{0}$. Mass transport of water will then only occur through the gas phase. Heat can flow through all three phases.

We assume gas flow at low Reynolds numbers and therefore choose to model the viscous friction force to be proportional to the gas flow velocity v^{g}_{k} and the gas viscosity η^{g},

$$\Theta^{g}_{k} = -\alpha^{g}\alpha^{g}\eta^{g}v^{g}_{k}/\kappa. \tag{20}$$

This choice of model defines the permeability κ of the insulation, where we have used $\kappa = 3\times10^{-10}\,\mathrm{m}^2$. We have used the value $\eta^{g} = 1.8\times10^{-5}\,\mathrm{Pa\,s}$ for the viscosity, 0.97 for the porosity and the constant value of $\lambda = 5.4\times10^{-2}\,\mathrm{W\,m^{-1}\,K^{-1}}$ for the overall thermal conductivity, defined as

$$\lambda \equiv \alpha^{g}\lambda^{g} + \alpha^{a}\lambda^{a} + \alpha^{s}\lambda^{s}. \tag{21}$$

In the momentum equation (4) for the gas phase, we assume instant relaxation to steady-state flow and neglect the contribution from $v^{i}_{k}\Psi^{g}$. Furthermore, the low Reynolds number assumption means that the inertial term can also be omitted. Equation (4) then reduces to Darcy's law.

Taking advantage of the cylindrical symmetry, the transport equations to be solved reduce to four partial differential equations (PDEs); the mass balances for water, oxygen and nitrogen, and a PDE for the energy balance (Eq. (6)). These were spatially discretized with the finite volume method (FVM) [59] on a one-dimensional grid with 40 uniform cells, producing a system of coupled ordinary differential equations (ODEs). The ODEs were integrated in time using the backward Euler method [60]. Each time step involved solving a system of non-linear equations using the Scalable Nonlinear Equations Solvers (SNES) component the PETSc library [61,62], with `fsolve` from the `optimize` module of SciPy [63] as a fallback.

Heat and mass fluxes were calculated by use of the force-flux relations (Eqs. (13)-(15)) using the Onsager coefficients calculated from RET, as described in Sec. 2.3 with $b_{ij} = 1$. We will compare two ways to compute the fluxes:

With Coupling All Onsager coefficients were used in the force-flux relations in Eqs. (13)-(15).

No Coupling All the cross-coefficients representing heat and mass coupling were set to zero, $L_{iq} = 0$.

However, all simulations were carried out **with** coupling included. The different ways to compute the fluxes were only used in the post-processing routine to estimate the influence of coupling on the magnitude of the fluxes.

3.2. The Soret coefficients of humid air

Humid air is represented as a ternary mixture of water, nitrogen and oxygen. When reporting the Soret coefficients of humid air, we adhere to the definition given by Ortiz de Zárate [64], which in the state of vanishing mass fluxes can be written as

$$\begin{pmatrix} S_{T,H_2O} \\ S_{T,O_2} \end{pmatrix} = -\frac{1}{\nabla T}\begin{bmatrix} x_{H_2O}(1-x_{H_2O}) & -x_{H_2O}x_{O_2} \\ -x_{H_2O}x_{O_2} & x_{O_2}(1-x_{O_2}) \end{bmatrix}^{-1}\begin{pmatrix} \nabla x_{H_2O} \\ \nabla x_{O_2} \end{pmatrix}, \tag{22}$$

where $S_{T,i}$ and x_i are the Soret coefficient and mole fraction of component i.

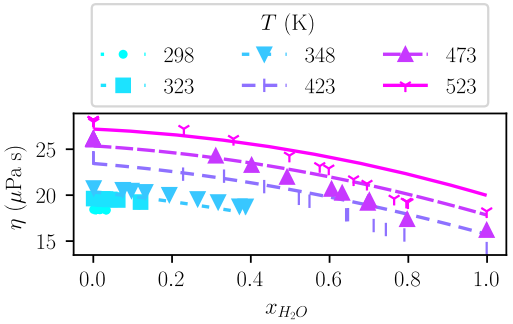

Fig. 2. The viscosity of humid air at 1 bar as predicted using RET-Mie (lines), measured for mixtures [65], and computed for pure fluids from correlations [66, 67] (symbols). The error in RET-Mie predictions is within - 3 % for pure air and + 15 % for pure water vapour, with AARD of 5.01 % for all data points.

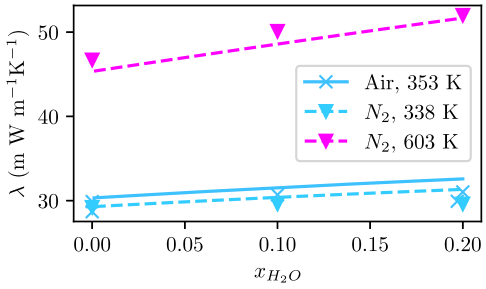

Fig. 3. Thermal conductivity of humid air and the water/nitrogen mixture at up to 1 bar as predicted using RET-Mie (lines), and measured (symbols) [68]. The error in predictions is $<$ 8.8 % for all experimental data points, with AARD 3.5 %. In comparison with the correlation by Lemmon and Jacobsen [66] for pure air, the deviation between RET-Mie and the correlation is $<$ 2.6 %, with AARD 1.4 %. For pure water, the deviation between RET-Mie and pure fluid correlations is up to 51 % for temperatures ranging from 375 K to 600 K.

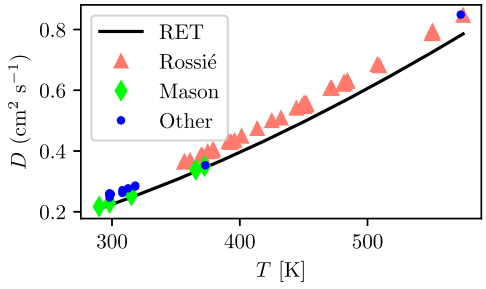

Fig. 4. The diffusion coefficient of water in air as predicted by RET-Mie at 1 bar, $x_{H_2O} = 1\%$ (line), and measured (symbols) [69–76]. The deviation in RET-Mie predictions from the data is within ± 14 %, with AARD 8.6 %. The smallest deviation is from the data set from Mason, with all errors within ± 2.5 %, and AARD 1.4 %.

4. Results and discussion

4.1. Comparison to experimental data on the transport properties of humid air

The RET-Mie presented in Sec. 2.3 requires input parameters for the Mie potentials to calculate transport properties. The thermodynamic properties of oxygen and nitrogen are represented to good accuracy by Mie-potentials, where we have used parameters from Refs. [77] and [78] respectively. The effects of internal degrees of freedom on the thermal conductivity were accounted for by using RET-Mie with the Eucken correction [79].

It has been shown in the literature that the Mie potential is capable of representing the transport properties of gas mixtures containing

Table 1
Parameters used with RET-Mie and values for water from Mason et al. [70].

Specie	σ (Å)	ϵ (k_B^{-1})	λ_r (-)	λ_a (-)	Ref.
H_2O	2.5466	706.67	9.0	6.0	This work
H_2O	2.71	506.0	12.0	6.0	[70]
O_2	3.46	118.0	12.0	6.0	[77]
N_2	3.609	105.79	14.08	6.0	[78]

Table 2
The average absolute relative deviation (%) from experimental data and reference correlations [66] obtained from the different parameter sets for water indicated in Table 1. Subscript mix refers to mixtures of humid air, and subscript H_2O refers to pure water.

Ref.	η_{H_2O}	η_{mix}	λ_{H_2O}	λ_{mix}	D
This work	10.04	5.01	47.88	3.54	8.65
[70]	24.48	7.51	67.24	4.15	7.14

water, provided that the water content is sufficiently low to suppress the relevance of dipole-dipole interactions [70,80]. Using experimental data for diffusion coefficients of water in nitrogen and air, the viscosity of humid air, and the thermal conductivity of humid air at mole fractions of water below 0.2 (to avoid the regime where dipole-dipole interactions are prevalent), we find that the parameters in the first row of Table 1 give, overall, the most accurate predictions. Relevant details on how the parameters for water were regressed can be found in the SI. For the case of water, we have also included for comparison values from Mason et al. [70], which are similar to those found in this work. Since the parameters from Mason et al. [70] were fitted with a Stockmayer potential, which also includes a dipole term, they are not expected to be exactly the same as for the Mie potential used in this work.

The resulting average absolute relative deviation (AARD) for the different parameter sets are shown in Table 2. The table shows that none of the parameter sets give accurate predictions of the thermal conductivity of pure water. However, for mixtures where the mole fraction of water is below 0.2, the transport properties of humid air can be represented within 10%.

Figs. 2, 3 and 4 compare predictions from RET-Mie to experimental data for the viscosity, thermal conductivity and diffusion coefficient of humid air. Details on how the binary diffusion coefficient of humid air was calculated based on the four diffusion coefficients of the ternary system can be found in the supporting information (SI). The figures illustrate that the temperature dependence of the transport properties of humid air are correctly captured by RET-Mie.

Fig. 2 shows that the deviation between experiments and RET-Mie increases as the mole fraction of water increases. The most recent data-set on experimental diffusion coefficients of humid air shown in Fig. 4 are from 1962 [75], while the oldest data-set is from 1934 [76]. The majority of the experimental data are located slightly above the predictions from RET-Mie with an AARD of 8.6%. The data-set by Mason however [70], lies right on top of the predictions from RET-Mie, with an AARD of 1.4%.

4.2. The Soret coefficients of humid air

RET-Mie has its basis in non-equilibrium statistical mechanics [49]. Moreover, the comparison with experiments in Sec. 4.1 shows that the theory reproduces the transport-properties of humid air mostly within 10%, and gives the right temperature and composition dependence provided that $x_{H_2O} < 0.2$. This supports the assumption that the theory should also give reliable predictions of Soret coefficients.

Fig. 5 shows the Soret coefficients of water and oxygen in humid air defined in Eq. (22), predicted by RET-Mie. In the inspected temperature and composition range, the Soret coefficient of water, S_{T,H_2O},

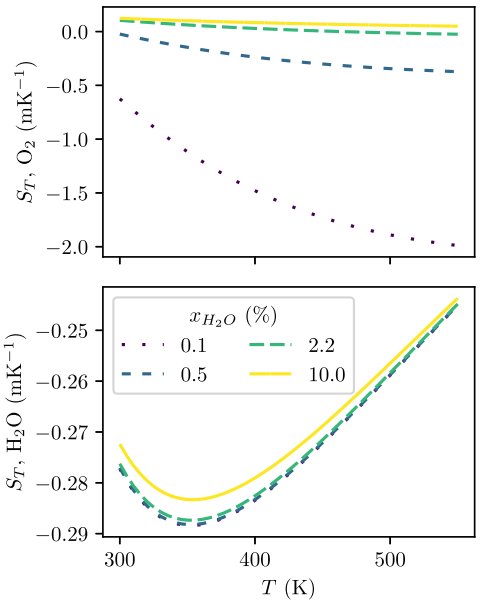

Fig. 5. The Soret coefficient of water and oxygen in humid air at 1 bar, as a function of temperature for several mole fractions of water. At all conditions, $x_{N_2}/x_{O_2} = 0.79/0.21$.

has a value of about -0.3 mK^{-1}. The Soret coefficient of oxygen, S_{T,O_2}, changes from positive at high mole fractions of water, to negative at smaller water concentrations.

It is evident from Eq. (22) that both Soret coefficients contribute to the redistribution of water in a large temperature gradient. Hence, to better understand the practical implications of these coefficients, we now investigate an example with exposure of humid air inside of an insulation material to a large temperature gradient.

4.3. A Case study of thermal diffusion in insulation materials

This section contains a discussion of the examples described in Sec. 3, where water redistributes in a 5 cm thick insulation material surrounding a cylindrical pipe as the insulation material is heated. Initially, the insulation material has a uniform temperature and composition profile. Then, at $t = 0$, the temperature at the western boundary (the pipe wall) is increased by 50 K, which leads to a redistribution of the water.

We will first discuss an example where we impose zero adsorption and desorption in the insulation material, setting $\Gamma(\mathrm{RH}) = 0$. The temperature and composition profiles during a simulation lasting 60 minutes are shown in Fig. 6. Figures 6a and 6b show that in 60 minutes, the temperature and composition profiles change from almost constant, to steady-state profiles matching the boundary conditions. By comparing the blue and the red dashed lines in Fig. 6b, it is evident that thermal diffusion leads to a mole fraction of water in the gas phase that is higher at the hot location than if thermal diffusion is neglected. However, the effect is relatively small, and the mole fraction of water increases from 0.00787 to 0.00799 at the warmest location, i.e. an increase of 1.5%. It is also interesting for this case to consider the diffusive mass fluxes, plotted in Fig. 6c, with and without thermal diffusion coupling (see Sec. 3). With coupling, the mass flux is a couple of orders of magnitude lower than if coupling is neglected. The Soret effect here counteracts the mass flux contributions from the gradients of the chemical potentials, and it is crucial to include coupling to achieve the correct magnitude of the mass flux.

In Fig. 7 we show the temperature, water mole fraction and mass flux profiles for the example if sorption is included. Although the temperature evolutions shown in Figs. 6a and 7a are very similar, the redistribution of moisture becomes fundamentally different with sorption. Since the adsorbed amount increases with increasing relative humid-

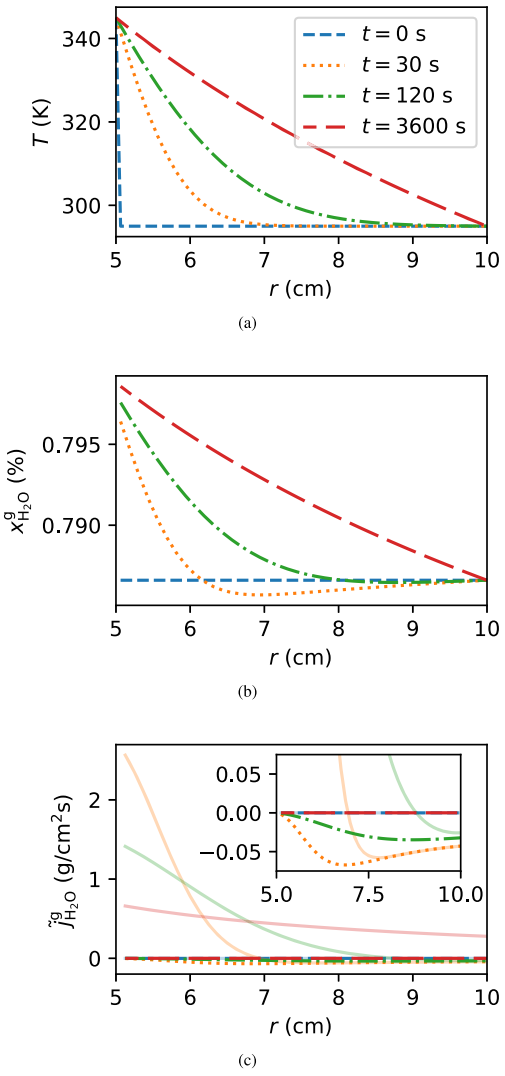

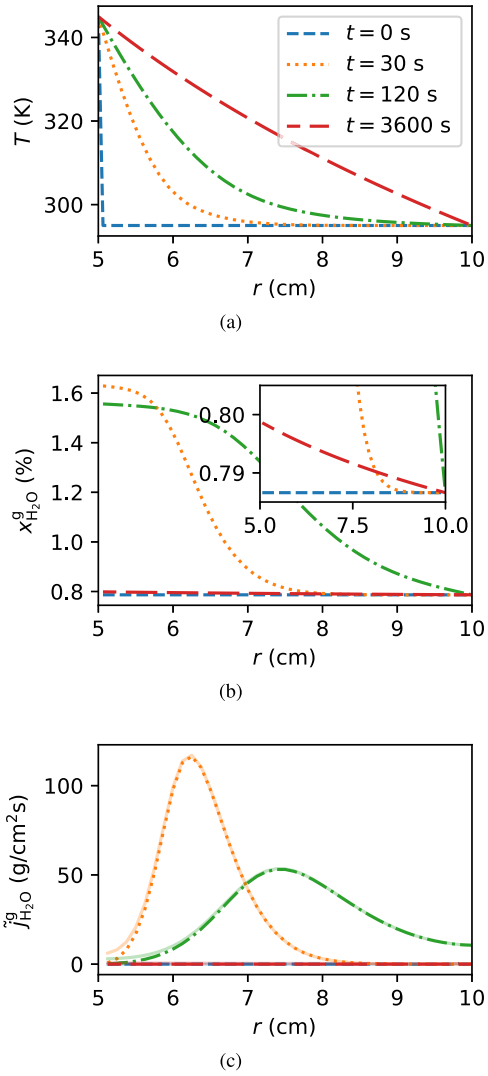

Fig. 6. Results from the warm-up case without sorption showing (a) temperature, (b) mole fraction of water in the gas phase and (c) diffusive flux of water in the gas phase at times 0 s (short-dashed blue), 30 s (dotted orange), 120 s (dash-dotted green) and 3600 s (long-dashed red). In (c), diffusive water fluxes computed without thermal diffusion ($L_{i,q} = 0$) are shown at times 0 s (semi-transparent blue), 30 s (semi-transparent orange), 120 s (semi-transparent green) and 3600 s (semi-transparent red). (For interpretation of the colors in the figure(s), the reader is referred to the web version of this article.)

Fig. 7. Results from the warm-up case with sorption showing (a) temperature, (b) mole fraction of water in the gas phase and (c) diffusive flux of water in the gas phase at times 0 s (short-dashed blue), 30 s (dotted orange), 120 s (dash-dotted green) and 3600 s (long-dashed red). In (c), diffusive water fluxes computed without thermal diffusion ($L_{i,q} = 0$) are shown at times 0 s (semi-transparent blue), 30 s (semi-transparent orange), 120 s (semi-transparent green) and 3600 s (semi-transparent red).

ity, and the relative humidity decays exponentially with temperature, a large desorption occurs at the hot end of the insulation material. The desorption manifests as an increase in the water mole fraction at the two intermediate times, $t = 30$ s and $t = 120$ s, before eventually the steady-state mole fraction ends up very similar as in Fig. 6 (see inset in Fig. 7b). In the case with adsorption, the overlapping dashed and solid lines in Fig. 7c mean that the thermal diffusion gives a much smaller contribution than the diffusion contribution from the gradients of the chemical potentials. Despite the much smaller magnitude of the coupling contribution to the mass flux, it results in a mole fraction of water in the gas phase that is about 1.5% higher at the hot location than if thermal diffusion is neglected, as shown in Fig. 7b.

5. Conclusion

The aim of this work has been to clarify to what extent thermal diffusion affects the migration of water in humid air through porous insulation materials.

No experimental measurements of the Soret coefficients of humid air could be found in the literature. As an alternative, Revised Enskog theory for Mie fluids (RET-Mie) was used to calculate the transport properties of humid air, which was represented as a ternary mixture of nitrogen, oxygen and water. It was found that Mie fluids were capable of representing the transport of properties of humid air, provided that the mole fraction of water remained below 0.2. At higher water mole fractions, dipole-dipole interactions influence the transport properties such that Mie potentials are insufficient to represent the fluid properties of the gas mixture.

Comparison to experimental data from literature showed that RET-Mie reproduces the diffusion coefficient, viscosity and thermal conductivity of humid air within 8.7%, 5.0% and 3.5% respectively. Moreover, the theory gives a temperature and composition dependence similar to the experimental values. This supports the assumption that the theory also gives reliable predictions of Soret coefficients. In the investigated composition and temperature range, RET-Mie predicted the Soret coefficient of water to be approximately $-0.3\,\mathrm{mK}^{-1}$, while the Soret coefficient of oxygen varied from $-1.2\,\mathrm{mK}^{-1}$ to $+0.1\,\mathrm{mK}^{-1}$.

To clarify the role of thermal diffusion in insulation materials, we investigated a case with heating of glass wool insulation containing humid air, which was surrounding a cylindrical pipe. Non-equilibrium thermodynamics was used to consistently incorporate the Soret coefficients into the flux equations in a dynamic, non-isothermal model that included diffusion, convection, thermal conduction and adsorption in the porous medium. At steady-state with 50 K temperature difference across 5 cm of insulation, thermal diffusion gave a mole fraction of water that was about 1.5% higher at the hot location than if thermal diffusion were neglected.

CRediT authorship contribution statement

Vegard G. Jervell: Writing – review & editing, Writing – original draft, Visualization, Validation, Software, Methodology, Investigation, Formal analysis. **Magnus Aa. Gjennestad:** Writing – review & editing, Writing – original draft, Visualization, Validation, Software, Investigation, Formal analysis, Conceptualization, Methodology. **Thuat T. Trinh:** Writing – review & editing, Software, Investigation, Formal analysis. **Øivind Wilhelmsen:** Investigation, Funding acquisition, Formal analysis, Conceptualization, Methodology, Project administration, Supervision, Validation, Writing – original draft, Writing – review & editing.

Declaration of competing interest

The authors declare that they have no known competing financial interests or personal relationships that could have appeared to influence the work reported in this paper.

Data availability

Data will be made available on request.

Acknowledgements

This work was supported by the PredictCUI project coordinated by SINTEF Energy Research, and the authors acknowledge the contributions of Equinor, Gassco, Shell and the Petromaks programme of the Research Council of Norway (308770). This work was partly supported by the Research Council of Norway through its Centres of Excellence funding scheme, Porelab, Project Number 262644.

Appendix A. Supplementary material

Supplementary material related to this article can be found online at https://doi.org/10.1016/j.ijheatmasstransfer.2024.125576.

References

[1] P. Tsilingiris, Thermophysical and transport properties of humid air at temperature range between 0 and 100 °C, Energy Convers. Manag. 49 (5) (2008) 1098–1110.
[2] T. Kuijten, Water Vapor Migration Through Insulation, 2016.
[3] P. Kosiński, P. Brzyski, B. Duliasz, Moisture and wetting properties of thermal insulation materials based on hemp fiber, cellulose and mineral wool in a loose state, J. Nat. Fibers 17 (2) (2020) 199–213, https://doi.org/10.1080/15440478.2018.1477086.
[4] G. Promis, L.F. Dutra, O. Douzane, A.T. Le, T. Langlet, Temperature-dependent sorption models for mass transfer throughout bio-based building materials, Constr. Build. Mater. 197 (2019) 513–525, https://doi.org/10.1016/j.conbuildmat.2018.11.212.
[5] R. Avramidis, Evaluation of “three-variable” models for the prediction of equilibrium moisture content in wood, Wood Sci. Technol. 23 (1989) 251–257, https://doi.org/10.1007/BF00367738.
[6] M. Jerman, R. Černý, Effect of moisture content on heat and moisture transport and storage properties of thermal insulation materials, Energy Build. 53 (2012) 39–46, https://doi.org/10.1016/j.enbuild.2012.07.002.
[7] J. Langmans, A. Nicolai, R. Klein, S. Roels, A quasi-steady state implementation of air convection in a transient heat and moisture building component model, Build. Environ. 58 (2012) 208–218.
[8] B. Song, L. Bai, L. Yang, Analysis of the long-term effects of solar radiation on the indoor thermal comfort in office buildings, Energy 247 (2022) 123499.
[9] B. Häussling Löwgren, J. Bergmann, O. Alves-Filho, A numerical implementation of the Soret effect in drying processes, ChemEngineering 4 (1) (2020) 13.
[10] H.S. Lee, W.W. Carr, H.W. Beckham, J. Leisen, A model of through-air drying of tufted textile materials, Int. J. Heat Mass Transf. 45 (2) (2002) 357–366.
[11] T. Lu, S. Shen, Numerical and experimental investigation of paper drying: Heat and mass transfer with phase change in porous media, Appl. Therm. Eng. 27 (8–9) (2007) 1248–1258.
[12] J. Kumberg, M. Mueller, R. Diehm, S. Spiegel, C. Wachsmann, W. Bauer, P. Scharfer, W. Schabel, Drying of lithium-ion battery anodes for use in high-energy cells: Influence of electrode thickness on drying time, adhesion, and crack formation, Energy Technol. 7 (11) (2019) 1900722.
[13] Q. Cao, T. Pojtanabuntoeng, M. Esmaily, S. Thomas, M. Brameld, A. Amer, N. Birbilis, A review of corrosion under insulation: A critical issue in the oil and gas industry, Metals 12 (4) (2022) 561.
[14] F. De Vogelaere, Corrosion under insulation, Process Saf. Prog. 28 (1) (2009) 30–35.
[15] Y.-H. Tsai, J. Wang, W.-T. Chien, C.-Y. Wei, X. Wang, S.-H. Hsieh, A BIM-based approach for predicting corrosion under insulation, Autom. Constr. 107 (2019) 102923.
[16] J.S. Rowlinson, B. Widom, Molecular Theory of Capillarity, Clarendon Press, Oxford, 1984.
[17] M.Aa. Gjennestad, Ø. Wilhelmsen, Thermodynamic stability of droplets, bubbles and thick films in open and closed pores, Fluid Phase Equilib. 505 (2020) 112351.
[18] M.Aa. Gjennestad, Ø. Wilhelmsen, Thermodynamic stability of volatile droplets and thin films governed by disjoining pressure in open and closed containers, Langmuir 36 (27) (2020) 7879–7893.
[19] L.J.T.M. Kempers, A comprehensive thermodynamic theory of the Soret effect in a multicomponent gas, liquid or solid, J. Chem. Phys. 115 (2001) 6330.
[20] J.P. Severinghaus, M.L. Bender, R.F. Keeling, W.S. Broecker, Fractionation of soil gases by diffusion of water vapor, gravitational settling, and thermal diffusion, Geochim. Cosmochim. Acta 60 (6) (1996) 1005–1018.
[21] P.-A. Artola, B. Rousseau, G. Galliéro, A new model for thermal diffusion: kinetic approach, J. Am. Chem. Soc. 130 (33) (2008) 10963–10969.
[22] R. Taylor, R. Krishna, Multicomponent Mass Transfer, John Wiley & Sons, Ltd., New York, 1992.
[23] R. Taylor, R. Krishna, Multicomponent Mass Transfer, vol. 2, John Wiley & Sons, 1993.
[24] S. Kjelstrup, D. Bedeaux, E. Johannessen, J. Gross, Non-Equilibrium Thermodynamics for Engineers, 2nd edition, World Scientific Co., 2017.
[25] W. Köhler, K.I. Morozov, The Soret effect in liquid mixtures - a review, J. Non-Equilib. Thermodyn. 41 (3) (2016) 151–197, https://doi.org/10.1515/jnet-2016-0024.
[26] C. Ludwig, Diffusion zwischen ungleich erwärmten Orten gleich zusammengesetzter Lösungen, Sitzber. Akad. Wiss. Wien Math.-Naturw. Kl. 20 (1856) 539.
[27] S. Kjelstrup, D. Bedeaux, Non-Equilibrium Thermodynamics of Heterogeneous Systems, 1st edition, World Scientific Co., Singapore, 2008.
[28] A. Firoozabadi, K. Ghorayeb, K. Shukla, Theoretical model of thermal diffusion factors in multicomponent mixtures, AIChE J. 46 (5) (2000) 892–900.
[29] H. Brenner, Elementary kinematical model of thermal diffusion in liquids and gases, Phys. Rev. E 74 (3) (2006) 036306.
[30] M.G. Gonzalez-Bagnoli, A.A. Shapiro, E.H. Stenby, Evaluation of the thermodynamic models for the thermal diffusion factor, Philos. Mag. 83 (17–18) (2003) 2171–2183.
[31] K.J. Zhang, M.E. Briggs, R.W. Gammon, J.V. Sengers, Optical measurement of the soret coefficient and the diffusion coefficient of liquid mixtures, J. Chem. Phys. 104 (17) (1996) 6881–6892, https://doi.org/10.1063/1.471355.
[32] J.K. Platten, M. Bou-Ali, P. Costesèque, J. Dutrieux, W. Köhler, C. Leppla, S. Wiegand, G. Wittko, Benchmark values for the Soret, thermal diffusion and diffusion coefficients of three binary organic liquid mixtures, Philos. Mag. 83 (17–18) (2003) 1965–1971.
[33] A.F. Bogatyrev, O.A. Makeenkova, M.A. Nezovitina, Experimental study of thermal diffusion in multicomponent gaseous systems, Int. J. Thermophys. 36 (2015) 633–647.
[34] B. Hafskjold, D. Bedeaux, S. Kjelstrup, Ø. Wilhelmsen, Soret separation and thermo-osmosis in porous media, Eur. Phys. J. E 45 (5) (2022) 41.
[35] M. Partha, P. Murthy, G. Raja Sekhar, Soret and Dufour effects in a non-Darcy porous medium, ASME J. Heat Mass Transf. 128 (6) (2006) 605–610.
[36] V.G. Jervell, Ø. Wilhelmsen, Revised Enskog theory for Mie fluids: Prediction of diffusion coefficients, thermal diffusion coefficients, viscosities, and thermal conductivities, J. Chem. Phys. 158 (22) (2023) 224101.
[37] H. Janssen, Thermal diffusion of water vapour in porous materials: Fact or fiction?, Int. J. Heat Mass Transf. 54 (7–8) (2011) 1548–1562.
[38] R. Peuhkuri, C. Rode, K.K. Hansen, Non-isothermal moisture transport through insulation materials, Build. Environ. 43 (5) (2008) 811–822.
[39] P.H. Baker, G.H. Galbraith, R.C. McLean, Temperature gradient effects on moisture transport in porous building materials, Build. Services Eng. Res. Technol. 30 (1) (2009) 37–48.
[40] M.Aa. Gjennestad, Ø. Wilhelmsen, Thermodynamically consistent modeling of adsorbed phases in porous media, Int. J. Heat Mass Transf. 226 (2024) 125462.

[41] B. Song, X. Wang, J. Wu, Z. Liu, Calculations of the thermophysical properties of binary mixtures of noble gases at low density from ab initio potentials, Mol. Phys. 109 (12) (2011) 1607–1615.
[42] F. Sharipov, V.J. Benites, Transport coefficients of isotopic mixtures of noble gases based on ab initio potentials, Phys. Chem. Chem. Phys. 23 (2021).
[43] F. Sharipov, V.J. Benites, Transport coefficients of helium-neon mixtures at low density computed from ab initio potentials, J. Chem. Phys. 147 (22) (2017).
[44] F. Sharipov, V.J. Benites, Transport coefficients of multi-component mixtures of noble gases based on ab initio potentials: viscosity and thermal conductivity, Phys. Fluids 32 (2020) 077104, https://doi.org/10.1063/5.0016261.
[45] F. Sharipov, V.J. Benites, Transport coefficients of multicomponent mixtures of noble gases based on ab initio potentials: Diffusion coefficients and thermal diffusion factors, Phys. Fluids 32 (2020) 097110, https://doi.org/10.1063/5.0025176.
[46] F. Sharipov, V.J. Benites, Transport coefficients of argon and its mixtures with helium and neon at low density based ab initio potentials, Fluid Phase Equilib. 498 (2019) 23–32.
[47] R. Hellmann, C. Gaiser, B. Fellmuth, T. Vasyltsova, E. Bich, Thermophysical properties of low-density neon gas from highly accurate first-principles calculations and dielectric-constant gas thermometry measurements, J. Chem. Phys. 154 (16) (2021).
[48] R. Hellmann, Cross second virial coefficients and dilute gas transport properties of the systems (N_2 + C_3H_8), (C_2H_6 + C_3H_8), and (H_2S + C_3H_8) from ab initio-based intermolecular potentials, J. Chem. Eng. Data 65 (9) (2020) 4712–4724.
[49] S. Chapman, T.G. Cowling, The Mathematical Theory of Non-uniform Gases, 3rd edition, Cambridge University Press, Bentley House, 200 Euston Road, London, N.W. 1, 1970.
[50] E.G.D. Cohen, Fifty years of kinetic theory, Phys. A, Stat. Mech. Appl. 194 (1) (1993) 229–257, https://doi.org/10.1016/0378-4371(93)90357-A, https://www.sciencedirect.com/science/article/pii/037843719390357A.
[51] M. López de Haro, E.G.D. Cohen, J.M. Kincaid, The Enskog theory for multicomponent mixtures. I. Linear transport theory, J. Chem. Phys. 78 (5) (1983) 2746–2759.
[52] J. Kincaid, M. Lopez de Haro, E. Cohen, The Enskog theory for multicomponent mixtures. II. Mutual diffusion, J. Chem. Phys. 79 (9) (1983) 4509–4521.
[53] M. Lopez de Haro, E. Cohen, The Enskog theory for multicomponent mixtures. III. Transport properties of dense binary mixtures with one tracer component, J. Chem. Phys. 80 (1) (1984) 408–415.
[54] J. Kincaid, E. Cohen, M. Lopez de Haro, The Enskog theory for multicomponent mixtures. IV. Thermal diffusion, J. Chem. Phys. 86 (2) (1987) 963–975.
[55] V.G. Jervell, ThermoTools: KineticGas, https://github.com/thermotools/KineticGas, 2023.
[56] S. Brunauer, P.H. Emmett, E. Teller, Adsorption of gases in multimolecular layers, J. Am. Chem. Soc. 60 (2) (1938) 309–319, https://doi.org/10.1021/ja01269a023.
[57] T.L. Hill, Statistical mechanics of multimolecular adsorption. I, J. Chem. Phys. 14 (4) (1946) 263–267, https://doi.org/10.1063/1.1724129.
[58] L. Marmoret, F. Collet, H. Beji, Moisture adsorption in glass wool products, High Temp., High Press. 40 (2011).
[59] R.J. LeVeque, Finite Volume Methods for Hyperbolic Problems, Cambridge Texts in Applied Mathematics, vol. 31, Cambridge University Press, New York, USA, 2002.
[60] E. Süli, D.F. Mayers, An Introduction to Numerical Analysis, Cambridge University Press, Cambridge, UK, 2003.
[61] S. Balay, S. Abhyankar, M.F. Adams, S. Benson, J. Brown, P. Brune, K. Buschelman, E.M. Constantinescu, L. Dalcin, A. Dener, V. Eijkhout, J. Faibussowitsch, W.D. Gropp, V. Hapla, T. Isaac, P. Jolivet, D. Karpeev, D. Kaushik, M.G. Knepley, F. Kong, S. Kruger, D.A. May, L.C. McInnes, R.T. Mills, L. Mitchell, T. Munson, J.E. Roman, K. Rupp, P. Sanan, J. Sarich, B.F. Smith, S. Zampini, H. Zhang, H. Zhang, J. Zhang, PETSc Web page, https://petsc.org/, 2023.
[62] L.D. Dalcin, R.R. Paz, P.A. Kler, A. Cosimo, Parallel distributed computing using Python, Adv. Water Resour. 34 (9) (2011) 1124–1139, https://doi.org/10.1016/j.advwatres.2011.04.013.
[63] P. Virtanen, R. Gommers, T.E. Oliphant, M. Haberland, T. Reddy, D. Cournapeau, E. Burovski, P. Peterson, W. Weckesser, J. Bright, S.J. van der Walt, M. Brett, J. Wilson, K.J. Millman, N. Mayorov, A.R.J. Nelson, E. Jones, R. Kern, E. Larson, C.J. Carey, İ. Polat, Y. Feng, E.W. Moore, J. VanderPlas, D. Laxalde, J. Perktold, R. Cimrman, I. Henriksen, E.A. Quintero, C.R. Harris, A.M. Archibald, A.H. Ribeiro, F. Pedregosa, P. van Mulbregt, SciPy 1.0 Contributors, SciPy 1.0: fundamental algorithms for scientific computing in Python, Nat. Methods 17 (2020) 261–272, https://doi.org/10.1038/s41592-019-0686-2.
[64] J.M. Ortiz de Zárate, Definition of frame-invariant thermodiffusion and Soret coefficients for ternary mixtures, Eur. Phys. J. E 42 (4) (2019) 1–8.
[65] J. Kestin, J. Whitelaw, The viscosity of dry and humid air, Int. J. Heat Mass Transf. 7 (11) (1964) 1245–1255.
[66] E.W. Lemmon, R.T. Jacobsen, Viscosity and thermal conductivity equations for nitrogen, oxygen, argon, and air, Int. J. Thermophys. 25 (1) (2004) 21–69.
[67] E.W. Lemmon, I.H. Bell, M.L. Huber, M.O. McLinden, NIST Chemistry WebBook, in: P.J. Linstrom, W.G. Mallard (Eds.), NIST Standard Reference Database, 69th edition, National Institute of Standards and Technology, Gaithersburg MD, 20899, 2023.
[68] A. Melling, S. Noppenberger, M. Still, H. Venzke, Interpolation correlations for fluid properties of humid air in the temperature range 100 °C to 200 °C, J. Phys. Chem. Ref. Data 26 (4) (1997) 1111–1123.
[69] K. Rossié, Die Diffusion von Wasserdampf in Luft bei Temperaturen bis 300 °C, Forsch. Geb. Ing.wes. (Ausg. A) 19 (2) (1953) 49–58.
[70] E.A. Mason, L. Monchick, Transport properties of polar-gas mixtures, J. Chem. Phys. 36 (10) (1961) 2746–2757.
[71] C.Y. Lee, C.R. Wilke, Measurements of vapor diffusion coefficient, Ind. Eng. Chem. 46 (11) (1954) 2381–2387, https://doi.org/10.1021/ie50539a046.
[72] E.T. Nelson, The measurement of vapour diffusivities in coal-gas and some common gases, J. Appl. Chem. 6 (7) (1956) 286–292, https://doi.org/10.1002/jctb.5010060704, https://onlinelibrary.wiley.com/doi/pdf/10.1002/jctb.5010060704, https://onlinelibrary.wiley.com/doi/abs/10.1002/jctb.5010060704.
[73] D.D. Kimpton, F.T. Wall, Determination of diffusion coefficients from rates of evaporation, J. Phys. Chem. 56 (6) (1952) 715–717, https://doi.org/10.1021/j150498a013.
[74] K.J. Brookfield, H.D.N. Fitzpatrick, J.F. Jackson, J.B. Matthews, E.A. Moelwyn Hughes, A.R. Todd, The escape of molecules from a plane surface into a still atmosphere, Proc. R. Soc. Lond. Ser. A, Math. Phys. Sci. 190 (1020) (1947) 59–67, https://doi.org/10.1098/rspa.1947.0061, https://royalsocietypublishing.org/doi/pdf/10.1098/rspa.1947.0061, https://royalsocietypublishing.org/doi/abs/10.1098/rspa.1947.0061.
[75] D.F. Othmer, H.T. Chen, Correlating diffusion coefficients in binary gas systems. use of viscosities in a new equation and nomogram, Ind. Eng. Chem. Process Des. Dev. 1 (4) (1962) 249–254, https://doi.org/10.1021/i260004a003.
[76] E.R. Gilliland, Diffusion coefficients in gaseous systems, Ind. Eng. Chem. 26 (6) (1934) 681–685, https://doi.org/10.1021/ie50294a020.
[77] J. Nichele, C.R. Abreu, L.S. de, B. Alves, I. Borges, Accurate non-asymptotic thermodynamic properties of near-critical N_2 and O_2 computed from molecular dynamics simulations, J. Supercrit. Fluids 135 (2018) 225–233.
[78] H. Hoang, S. Delage-Santacreu, G. Galliero, Simultaneous description of equilibrium, interfacial, and transport properties of fluids using a Mie chain coarse-grained force field, Ind. Eng. Chem. Res. 56 (32) (2017) 9213–9226.
[79] M.L. Huber, Thermal Conductivity, and Surface Tension of Selected Pure Fluids as Implemented in Refprop v10.0, 2018.
[80] S. Herrmann, H.-J. Kretzschmar, V.C. Aute, D.P. Gatley, E. Vogel, Transport properties of real moist air, dry air, steam, and water, Sci. Technol. Built Environ. 27 (4) (2021) 393–401.